Paramagnetic colloids: Chaotic routes to clusters and molecules

Hamed Abdi, Rasam Soheilian, Randall M. Erb, and Craig E. Maloney
Northeastern University, Boston, Massachusetts 02115, USA

(Received 2 November 2017; published 2 March 2018)

We present computer simulations and experiments on dilute suspensions of superparamagnetic particles subject to rotating magnetic fields. We focus on chains of four particles and their decay routes to stable structures. At low rates, the chains track the external field. At intermediate rates, the chains break up but perform a periodic (albeit complex) motion. At sufficiently high rates, the chains generally undergo chaotic motion at short times and decay to either closely packed clusters or more dispersed, colloidal molecules at long times. We show that the transition out of the chaotic states can be described as a Poisson process in both simulation and experiment.

DOI: 10.1103/PhysRevE.97.032601

I. INTRODUCTION

Guiding the assembly of paramagnetic particles by applying magnetic fields has become a popular technique for applications in biotechnology, photonics, composites, and other areas. Under static fields, the particles tend to form chains aligned along the direction of the applied field. The current generation of so-called superparamagnetic particles have very large magnetic susceptibilities, and with very moderate external fields on the order of a few mT, the chains are strong enough to overcome the Brownian drive. Early work in the 1990s focused on the dynamics—breakup and reformation—of these chains subject to shear flow and their impact on the rheological properties of the suspensions [1]. More recently, there has been interest in the effects of time-varying fields [2–29]. In general the design space for modulating the external field to obtain desired structures is quite rich and has only relatively recently begun to have been explored systematically [14]. Some driving protocols modulate the amplitude of the field along a fixed axis, with the extreme case being a pulsed on-off mode [30,31]. In others the field is kept at constant magnitude and rotated in a single plane [7,8,15–17,21–24,32–38].

When the field rotates in a plane, there is a tendency for particles to organize into lamellar structures and then to organize within the lamellae [5,6,14,39]. If the magnetostatic forces are much larger than the Brownian ones, they will control structure formation. However, even in the non-Brownian case, one observes a complex nonequilibrium phase behavior depending on the volume fraction of particles and the protocol for field rotation. If the field is left on for some time in some particular direction, particles begin to form chains. The chains grow and can coalesce. If the field is then reoriented, at sufficiently high volume fraction, the chains will collide and interact. At low enough volume fraction, they rotate without interacting significantly with each other.

Much of the early work on in-plane rotating fields focused on the breakup of individual chains at low volume fraction and high rotation rates [7,8,15–17,21–24,32–38]. At low rotation rates, a chain rotates with the field as a rigid body. It assumes a shape which becomes increasingly nonlinear as the rotation rate increases [17]. If the field is rotated sufficiently rapidly, the hydrodynamic forces on the chains will be too large relative to the magnetic forces, and the chain will break up. Previous work has gone into understanding and quantifying the initial breakup of the chain [7,8,17]. At the other side of the rotation rate spectrum, it is known that at very high rotation rates, the particles sample all possible field orientations before they have a chance to move appreciably. The magnetostatic interactions become effectively isotropic in this limit, and the chains collapse into closely packed planar structures: hexagonal crystals (or polycrystals) with some vacancies. However, the intermediate regime remains poorly understood.

In this paper, we focus on the dynamics of four-particle chains in the non-Brownian, athermal limit where the Brownian forces are neglected and the dynamics is controlled by the field rotation rate, Ω, alone. This is the simplest scenario, which gives rise to a rich and nontrivial dynamics at intermediate filed rotation rates. The relevant material parameters are the magnetic susceptibility, the particle size, and the viscosity of the suspending fluid. The two corresponding dimensionless groups are the Mason number, $\mathrm{Mn} = \Omega\tau_0$, and the characteristic dimensionless magnetic energy ϵ_0/k_bT, where (1) τ_0, is the characteristic time scale for viscous relaxation of a pair of particles in the suspending fluid under the characteristic (H_0-dependent) magnetostatic interaction forces, (2) k_bT is the thermal energy scale from the Brownian bath from the suspending fluid, and (3) ϵ_0 is the (H_0-dependent) characteristic magnetostatic energy for a pair of particles at contact. For the non-Brownian case, $k_bT/\epsilon_0 = 0$, we show that there exist three distinct dynamical regimes, separated by two well-defined bifurcation points, Mn_1 and Mn_2.

Below Mn_1, the chains rotate as a rigid body. The first transition at Mn_1 has been well studied by many other groups (for chains of various length) [17,38,40] and corresponds to the initial breakup of the chain due to the large hydrodynamic forces. For $\mathrm{Mn}_1 < \mathrm{Mn} < \mathrm{Mn}_2$, the chains fragment and reform in a completely periodic way. While the main chain is fragmented, each of the two subchains performs one complete rotation before reforming the main chain, and we call this motion a "do-si-do" in analogy with American square dancing. This periodic breakup and reformation of a single chain has already been observed and described in chains of arbitrarily

length by Melle and Martin [17]. At very large Mn, the magnetostatic interactions become effectively isotropic, and the chains quickly collapse into a closely packed configuration. This regime of very large Mn is also relatively well understood.

Our interest in this paper is the regime just above Mn_2. As $Mn \to Mn_2$ from below, the dynamics undergoes a saddle-node bifurcation. The frequency of the do-si-do motion, and the average magnetostatic energy, $\langle U_{MS} \rangle$, as functions of Mn, each develops a cusp at Mn_2, and the periodic do-si-do orbits discovered by Melle and Martin become unstable. Above the bifurcation, we observe a complex behavior in both experiments and simulations. The typical behavior of a trajectory in this regime is as follows. The system starts with a chaotic-like behavior, characterized by the transient largest Lyapunov exponent (LLE) defined below, with a broad temporal power spectrum. After some time (surprisingly long in both experiment and simulation) there is an abrupt transition from transient chaos into a periodic orbit with a well-defined fundamental frequency and essentially zero LLE indicating a return to nonchaotic dynamics. The structure in the final stable orbit is typically either (1) a closely packed cluster or (2) a structure with one of the four particles centered in an equilateral triangle composed of the other three. We refer to this latter orbit as a colloidal molecule [14,27,41,42]. Occasionally, we find other more complex periodic orbits with higher energy than either the closely packed clusters or triangular molecules, and we describe them in more detail below. Once formed, the final periodic orbits remain indefinitely stable. In both experiment and simulation, the survival probability of a trajectory remaining in the chaotic state is an exponential distribution, indicating that the transition from the chaotic regime into the final stable orbits can be considered to be a simple Poisson process.

The rest of this paper is organized as follows. In Sec. II we describe the model and protocols and the experimental setup. In Sec. III we discuss qualitatively the behaviors of typical trajectories in each of the regimes, $Mn < Mn_1$,$Mn_1 < Mn < Mn_2$, and $Mn > Mn_2$. In Sec. IV we use the average magneto-static energy in the final periodic orbit to define a phase diagram and discuss the transition dynamics out of chaotic states. Finally, in Sec. V we provide a summary and outlook.

II. NUMERICAL AND EXPERIMENTAL METHODS

We study the dilute suspension of paramagnetic colloids under external rotating magnetic fields. We specifically focus on chains of four particles since that is the shortest chain which shows a rich and nontrivial dynamics. We are interested in stable final structures at different rotation rates and the decay routes to them. We study the problem both computationally and experimentally. In this section we describe our computational and experimental methods.

A. Computational model

1. Dimensional analysis

Material parameters are particle size, a, fluid viscosity, η, particle susceptibility, χ, and room temperature, k_bT. Our control parameters are magnetic field strength, H_0, and field rotation rate, Ω. One can form a single energy scale, ϵ_0, out of these parameters. We choose it conventionally to be the total dipole-dipole interaction energy at contact: $\epsilon_0 = \mu_0 m_0^2/\pi a^3$ where $m_0 = H_0(\pi a^3/6)\frac{3\chi}{\chi+3}$ is the dipole moment of a lone particle in the external field and μ_0 is the vacuum permeability. One can then form a single time scale, $\tau_0 = 2ba^2/3\epsilon_0$, out of ϵ_0 where b is the Stokes drag coefficient. The two dimensionless groups controlling the response are the so-called Mason number, $Mn = \Omega\tau_0$, and the dimensionless Brownian drive, k_bT/ϵ_0. In the non-Brownian limit where $k_bT \ll \epsilon_0$, we are free to adjust both the field strength and fluid viscosity to tune τ_0, and we typically choose τ_0 to be on the order of a second in the experiments. In the rest of this paper, we present energies in units of ϵ_0, forces in units of $F_0 = \frac{3\epsilon_0}{4a}$, and times in units of $2\pi/\Omega$ unless stated otherwise.

2. Equations of motion

In general, in the overdamped regime, particles in a suspension must obey

$$F^M_{i\alpha} + F^C_{i\alpha} + F^H_{i\alpha} + F^R_{i\alpha} = 0_{i\alpha}, \quad (1)$$

where $F^M_{i\alpha}$, $F^C_{i\alpha}$, $F^H_{i\alpha}$, and $F^R_{i\alpha}$ are, respectively, the αth Cartesian component of the magnetostatic, contact, hydrodynamic, and random Brownian force and torque on the ith particle. F^M, F^C, and F^R depend on the configuration of all the particles, and F^H depends on both the configuration of all the particles and their velocities and rotation rates. Requiring the velocities and rotation rates to satisfy force balance at each configuration defines, implicitly, a first order dynamical system which can be integrated in time to calculate trajectories. A full treatment of F^M and F^H would require solving the Maxwell and Stokes equations subject to the appropriate boundary conditions at the particle surfaces, and approximation schemes have been developed for both F^M and F^H [8,40,43–47]. Following previous studies [17], we assume that, first, the particles act magnetostatically as point dipoles with moments slaved to the external field, independently of the other dipoles. This is a valid assumption at low values of χ where the pairwise dipole interactions dominate the multibody interactions. The particles that we use in our experiments have a relatively low susceptibility ($\chi = 0.512$). Therefore,

$$F^M_{i\alpha} = \sum_{j\neq i}^{N} F_0 \frac{a^4}{r_{ij}^4}[(3\cos^2\phi_{ij} - 1)\hat{r}_{ij\alpha} + \sin(2\phi_{ij})\hat{\theta}_{ij\alpha}], \quad (2)$$

where ϕ_{ij} is the phase lag between the external field vector H_0 and the separation vector r_{ij}, and $\hat{r}_{ij\alpha}$ and $\hat{\theta}_{ij\alpha}$ are the αth Cartesian component of the radial and tangential unit vectors, respectively. Second, the hydrodynamic drag on each particle is equal to that of an isolated particle in an infinite medium (i.e., Stokes drag model), $F^H_{i\alpha} = -bv_{i\alpha}$ where $b = 3\pi\eta a$. We ran simulations including far-field hydrodynamics and near-field lubrication interactions which suggested that Stokes drag model captures the essential physics of the problem. For F^C, to approximate the hard sphere condition, we take a simple pairwise power-law repulsion with an exponent of 36, $F^C_{i\alpha} = -F_0\sum_{j\neq i}^{N}(\frac{a}{r_{ij}})^{36}\hat{r}_{ij\alpha}$. Also, we take $F^R_{i\alpha} = 0_{i\alpha}$ as we focus on the non-Brownian case. We use the simple forward Euler method to integrate the velocities. For the case of

Stokes drag, solving for the velocities is trivial, and one has a simple closed-form expression for the velocity in terms of the configuration. The initial condition is a straight chain of particles in nominal contact with initial phase lag of ϕ_0. We systematically vary ϕ_0 at various Mn to study the dependence on initial conditions.

3. Tangent analysis of chaotic motion

To quantify the chaotic properties of the trajectories, we integrate the so-called tangent dynamics. Tangent dynamics, a standard analysis tool in dynamical systems theory [48], is defined by evolving an infinitesimally perturbed copy, $x'_{i\alpha} = x_{i\alpha} + \epsilon_{i\alpha}$, of the unperturbed system, $x_{i\alpha}$, according to the velocities obtained by linearizing the equations of motion about the true trajectory:

$$\frac{d}{dt}\epsilon_{i\alpha} = \sum_{j\beta} J_{i\alpha j\beta}\epsilon_{j\beta}, \tag{3}$$

where

$$J_{i\alpha j\beta} = \frac{\partial v_{i\alpha}}{\partial x_{j\beta}} \tag{4}$$

is the first derivative of the velocities with respect to the configuration, the so-called Jacobian matrix of the underlying system, and it is supposed to be evaluated at the actual underlying solution to the unperturbed system. In short, J tells us how perturbations to the underlying trajectory would grow in time: in general, positive eigenvalues of J give rise to diverging trajectories, while a lack of any positive eigenvalue means that nearby trajectories cannot diverge. For example, in the present case of non-Brownian Stokes drag, the underlying equations of motion read $v_{i\alpha} = \frac{1}{b}(F^M_{i\alpha} + F^C_{i\alpha})$, and $F^M_{i\alpha} + F^C_{i\alpha}$ is the configuration-dependent magnetostatic plus contact force. Then the Jacobian entries are simply the derivatives of the potential forces with respect to the particle positions $J_{i\alpha j\beta} = \frac{1}{b}\frac{\partial(F^M_{i\alpha}+F^C_{i\alpha})}{\partial x_{j\beta}}$. We have used an automated symbolic calculus package, Mathematica 10.0, to obtain closed form analytical expressions for $J_{i\alpha j\beta}$; they are not enlightening, and we do not reproduce them here. Our algorithm to evaluate $J_{i\alpha j\beta}$ scales like $O(N^2)$ and so is no more costly than the algorithm to evaluate the dipole forces themselves. We simply use forward Euler to evolve ϵ concurrently with the true underlying trajectory. In chaos theory [49–51], the Lyapunov spectrum is defined by the long-time average behavior of ϵ. In particular, the largest Lyapunov exponent (LLE) is defined as the long-time average of the derivative of $\log(|\vec{\epsilon}|)$ with respect to time. We show below that our trajectories exhibit increasing $\log(|\vec{\epsilon}|)$ during chaotic episodes before transitioning into stable orbits where $\log(|\vec{\epsilon}|)$ remains fixed. This is reminiscent of so-called transient chaotic behavior in damped systems [51].

B. Materials and experimental setup

Figure 1(a) shows a schematic of the experimental setup. Magnetic fields are applied using two 10 cm diameter iron-core solenoids that are placed in x and y directions creating dynamic magnetic fields $H_x = H_0 \cos\Omega t$ and $H_y = H_0 \sin\Omega t$, respectively. As a result, the resultant magnetic field has the constant magnitude of H_0 and rotates in the xy plane with angular velocity of Ω. The solenoids are fed with current from two

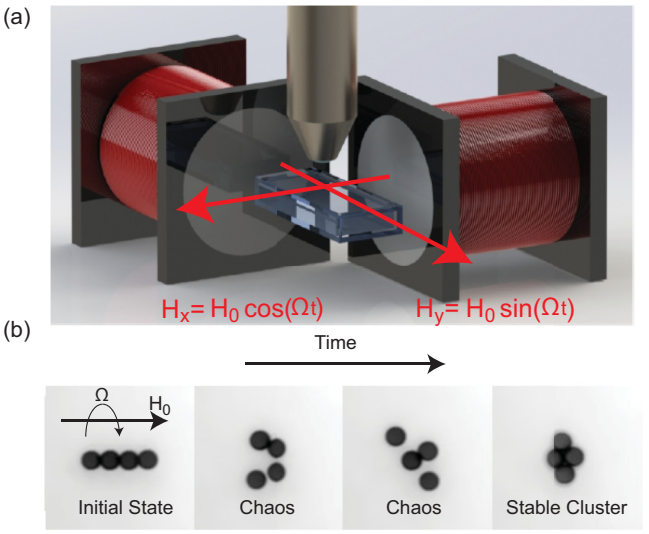

FIG. 1. (a) Schematic of the experimental setup. Two iron-core solenoids are used to create a magnetic field with constant magnitude of H_0, which rotates in the xy plane with angular velocity of Ω with an optical microscope imaging the xy plane. (b) Snapshots from a typical trajectory in experiments at Mn > Mn_2. In this regime, the short-time behavior is chaotic motion, and the long-time behavior is a stable periodic orbit. In this case, the final stable periodic orbit is a rotating closely packed cluster.

20-5M bipolar operational amplifiers (Kepco) controlled with a LabView program. Magnetic fields generated were measured using a 425 gaussmeter (Lake Shore Cryotronics Inc.). The utilized magnetic field is a homogeneous rotating magnetic field that has a magnitude of 10 mT.

Dilute suspensions of 2.8 μm M-270 Carboxylic Acid Dynabeads (Invitrogen, $\chi = 0.512$) were utilized for these experiments. Magnetic susceptibility indicated was determined using a superconducting quantum interference device magnetometer (Quantum Design Inc.). The particles were initially in aqueous suspensions and were added volumetrically to water-glycerol solutions for reaching desired viscosities ($\eta = 0.0446$ Pa · s).

Optical microscopy (custom column-mounted Nikon, Zyla Andors CMOS camera) was utilized to image the bead chains in real time. A fluid cell with a thickness of 500 μm was used for observing the bead suspension. Bead chains that were away from the surface of the substrate were studied in order to avoid surface interactions. Low exposure times were used to track particles over time, and videos were taken with 10–20 ms time steps. Videos were analyzed using the particle-tracking module of Fiji image analysis software. The magneto-static energy of the cluster was estimated by assuming a nominal magnetization of each bead and using a dipole approximation (as in the simulation code), $U_{MS} = \sum_{i=1}^{N}\sum_{j\neq i}^{N}\frac{a^3}{4r_{ij}^3}(1 - 3\cos^2\phi_{ij})$.

III. TYPICAL TRAJECTORIES

A. Configurations

We highlight our most significant result before fully describing the dynamics in different regimes of Mn. Figure 1(b) shows snapshots at various times from a typical trajectory in experiments just above Mn_2, which is where the literature

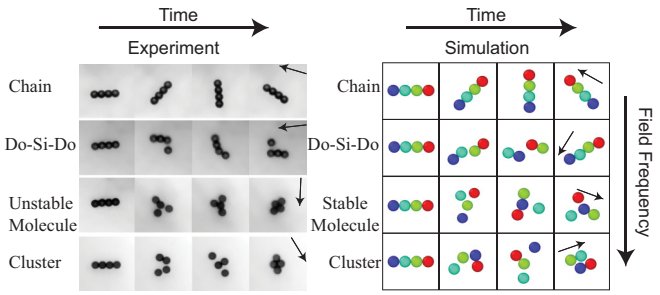

FIG. 2. Snapshots from typical trajectories in (left) experiments and (right) simulations. Particles are colored arbitrarily in the simulation to indicate identity. Time increases from left to right, and Mn increases from top to bottom. Field direction is shown in the rightmost columns.

lacks a clear description of the dynamics. It turns out the short-time response of the chain is a transient chaotic motion where symmetry breaks and particles exhibit an unpredictable motion. However, the long-time response is a periodic and indefinitely stable motion. In this example, the the long-time response is a closely packed colloidal cluster which rotates like a rigid body in the direction of the field but with an angular velocity different from Ω.

In Fig. 2 we show snapshots at various times for typical experiment (left) and simulation (right) trajectories. Mn increases from top to bottom. The first row corresponds to $\mathrm{Mn} < \mathrm{Mn}_1$ where the chain rotates as a (not quite linear) rigid body [17]. The second row corresponds to $\mathrm{Mn}_1 < \mathrm{Mn} < \mathrm{Mn}_2$ where there is a precisely periodic breakup and reformation of the chain. Each subchain roughly follows the orientation of the field before reformation of the main chain. Note that in the experiment, particle-to-particle variations in the magnetization and/or hydrodynamic radius may (and do) cause the periodic breakup and reformation during the do-si-do to occur at a site away from the center of the chain. Despite the broken symmetry, we see a periodic do-si-do regime for $\mathrm{Mn}_1 < \mathrm{Mn} < \mathrm{Mn}_2$ in the experiment. Movies $S1a$ and $S1b$ of the Supplemental Material [52] correspond to the do-si-do motion from simulation and experiment, respectively.

The third and fourth rows of Fig. 2 correspond to typical trajectories above Mn_2. The bifurcation at Mn_2 can be understood in terms of independent stability of each of the two subchains. If we treat each of the subchains independently, one would expect an instability above $\mathrm{Mn} = 1$. In practice, we find the location of the bifurcation point to be near but slightly below $\mathrm{Mn} = 1$ and can attribute this to the interaction between the two subchains facilitating the breakup. In this $\mathrm{Mn} > \mathrm{Mn}_2$ regime, the particles initially undergo a chaotic motion (to be made precise below) which, depending on the value of Mn, can last for many thousands of field revolutions before finally settling into a periodic orbit with a nontrivial orbital period not simply related to Ω. Typical configurations taken from the final periodic orbits are shown in the rightmost column of Fig. 2. There are two typical types of periodic orbits (with some exceptional cases discussed below) found after the chaotic dynamics. First, there is something like a closely packed planar cluster which undergoes topology changes in the contact network. This is shown in the bottom right row of Fig. 2. In this orbit, there will be periodic neighbor changes during which the cyan-blue contact will open in favor of the green-red contact, which will close. The cluster also simultaneously undergoes what is essentially a rigid body rotation. Movies $S2a$ and $S2b$ of the Supplemental Material [52] correspond to the cluster formation from simulation and experiment, respectively. Second, there is a more open kind of colloidal molecule. This is shown in the second row from the bottom of Fig. 2. In this orbit, one particle (colored blue in the figure) sits in the center and three others orbit it, forming what is essentially an equilateral triangle. The central particle follows a trajectory which is approximately an inscribed equilateral triangle. Each time the external field aligns with one of the three edges of the outer triangle, the central particle injects itself between the two and forms an almost-straight trimer aligned almost (with a slight lag) along the field axis. For example, in the configuration shown in the rightmost column of the second to last row, the central blue particle makes a trimer with the red and green particles on the outsides, and this trimer is almost aligned along the field direction but lags slightly behind. Later, the blue particle will inject itself between the red and cyan when the field is almost aligned along the red-cyan edge of the outer triangle. Movies $S3a$ and $S3b$ of the Supplemental Material [52] correspond to the molecule formation from simulation and experiment, respectively. Although we observe the transition from a chaotic regime to a stable periodic orbit in both experiment and simulation, the only final periodic orbits we have observed in the experiment have been the closely packed clusters. We believe this is due to the relatively high Mn where we currently operate the experiments and/or the disorder in particles' properties and will discuss this below.

B. Time series analysis

In Fig. 3 we perform a detailed analysis of the time series of the instantaneous magnetostatic energy, U_{MS}, in both the simulation and experiment for nonchaotic do-si-do states (a and b) at $\mathrm{Mn}_1 < \mathrm{Mn} < \mathrm{Mn}_2$, and chaotic states (c and d) at $\mathrm{Mn} > \mathrm{Mn}_2$; $t = 0$ corresponds to the moment at which the field begins to precess. Note that below Mn_1, U_{MS} is constant in both experiments and simulations since the chain rotates with a fixed phase angle relative to the external field. For the do-si-do, U_{MS} is almost perfectly periodic in both the experiment and simulation as shown in Figs. 3(a) and 3(b). For the chaotic case in Figs. 3(c) and 3(d), the power spectrum is computed only over the chaotic part of the signal excluding the periodic response. The power spectrum of both cases is noisy with no obvious peak. In the simulations, the system initially starts in a do-si-do-like periodic orbit. However, we find the initial periodic orbit linearly unstable, and if we perturb these states with an arbitrarily small temperature, they revert to an initially chaotic behavior as seen in the experiments. Very abruptly at the end of the chaotic regime, both the experiment and simulation lock into a periodic orbit with nontrivial period.

C. Tangent dynamics

We find the tangent dynamics a very useful tool in quantifying the nonlinear dynamical behavior and transitions into the basin of attraction of a stable orbit. We perform a tangent

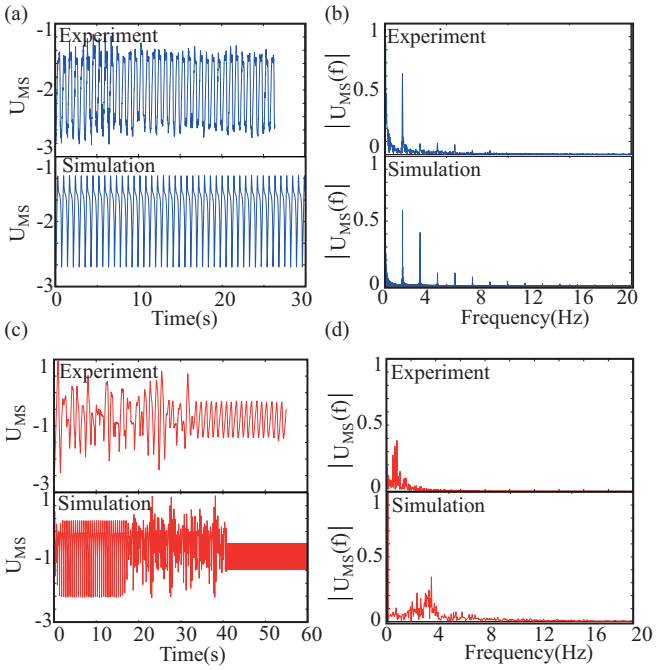

FIG. 3. (a) Magnetostatic energy, U_{MS}, and (b) its power spectrum for a typical trajectory with $\mathrm{Mn}_1 < \mathrm{Mn} < \mathrm{Mn}_2$. (c) Magnetostatic energy, U_{MS}, and (d) its power spectrum for a typical trajectory with $\mathrm{Mn} > \mathrm{Mn}_2$. For the experimental curves, U_{MS}, is inferred as described in the text, and the Fourier analysis is done only over the chaotic part.

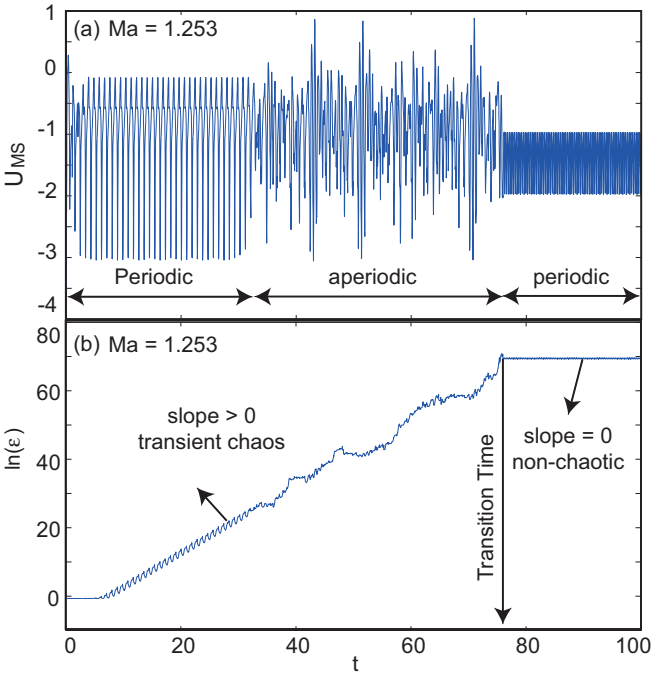

FIG. 4. For $\mathrm{Mn} = 1.253$ with $\phi_0 = 0$ (simulation result), (a) magnetostatic energy and (b) logarithm of the magnitude of the configuration space separation, $\log(|\vec{\epsilon}|)$ vs time.

dynamics analysis as described in Sec. II. Figures 4(a) and 4(b) show the instantaneous magnetostatic energy, U_{MS}, and the log of the phase space distance between the true trajectory and the tangent trajectory, $\log(|\vec{\epsilon}|)$, as functions of time. During the initial periodic motion, $\log(|\vec{\epsilon}|)$ grows indicating the linear instability of that periodic orbit. This periodic motion has a high degree of symmetry and is something like the do-si-do. After about 40 field revolutions, the symmetry breaks down, the trajectory becomes nonperiodic, and $\log(|\vec{\epsilon}|)$ continues to grow. The average slope of the $\log(|\vec{\epsilon}|)$ versus time curve can be considered as a transient measure of the LLE. Eventually the $\log(|\vec{\epsilon}|)$ versus time curve becomes completely flat, indicating a zero value for the LLE, a cessation of the chaos and an emergence of periodic motion. The tangent dynamics provides a useful way to precisely define the transition from chaotic (where ϵ increases exponentially in time) to periodic motion (where ϵ remains constant). We determine the moment of transition into the periodic orbit as follows. At each $t > T_p$, if $|\log(|\vec{\epsilon}(t)|) - \log[|\vec{\epsilon}(t - T_p)|]| < \delta$, then the transition time is $t^\star = t - T_p$. We take $T_p = 200$ field revolutions and $\delta = 2$, which is approximately two times the amplitude of fluctuations of $\log(|\vec{\epsilon}|)$ in the final periodic regime. Both of these are somewhat arbitrary, and we have verified that our distribution of transition times (shown below) is insensitive to the precise values.

IV. POPULATION DYNAMICS

At the end of the chaotic state the system finds itself in one of the possible final periodic orbits. In Fig. 5 we show the long-time averaged magnetostatic energy, $\langle U_{MS} \rangle$, versus Mn corresponding to the final periodic orbits. We consider $\langle U_{MS} \rangle$ to be a kind of order parameter indicating what dynamical state the system lives in. The two bifurcations at Mn_1 and Mn_2 are apparent. The leading nonanalytic behavior of $\langle U_{MS} \rangle$ on approach to both Mn_1 and Mn_2 can be described by a saddle-node bifurcation where $U - U_{1(2)} \propto \sqrt{(\mathrm{Mn} - \mathrm{Mn}_{1(2)})}$ where U_1 (or U_2) is the value at the bifurcation point [53]. Above Mn_2, there are two branches present. The higher branch corresponds to the molecule, while the lower one corresponds to the cluster. It is essential to try to understand the transition rates into and associated populations of these branches at

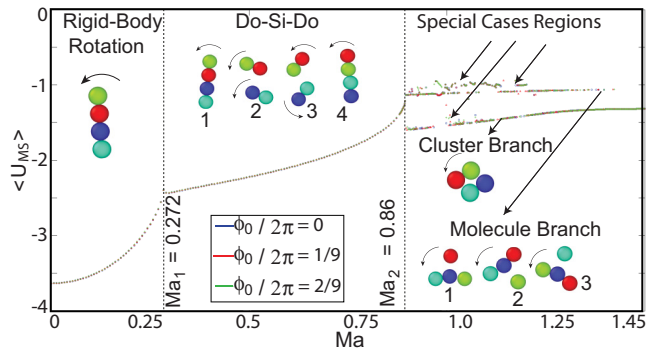

FIG. 5. Long-time-averaged magnetostatic energy, $\langle U_{MS} \rangle$, vs Mn (simulation result). ϕ_0 is the initial phase lag between the field direction and the chain orientation. Mn_1 and Mn_2 are the first and the second bifurcation points beyond which the rigid body rotation and the do-si-do motion become unstable, respectively. Above Mn_2, the typical dynamics consists of an episode of chaotic motion which eventually decays into a rotating colloidal cluster or molecule.

various Mn. Our results indicate that these populations have a very nonsmooth dependence on Mn, and a full study of the populations at various Mn and the associated transition rates is currently ongoing.

At very high Mn, the only remaining populated state is the cluster. This is to be expected since, in that regime, the field precesses many times before the particles are able to move appreciably, and the magnetostatic interactions average over all angles and become effectively isotropic.

There are ranges of Mn where one branch is suppressed while the other is populated. There are also two special cases which deserve mention. The first kind of special case is an island of stability in the Mn range where the initial do-si-do-like periodic orbits turn out to be stable, and the system remains in them forever without experiencing any chaotic behavior. One such regime is for Mn between 0.92 and 0.96. The second kind of special case is simply a third kind of terminal periodic orbit which competes with the cluster and molecule. For the Mn for which such a third terminal orbit is observed, the populations in each of the three grow exponentially in time as shown below. In this sense it is essentially no different from a cluster or molecule. Structurally, these orbits consist of two closely coupled dimers, neither of which ever break, aligned asymmetrically with the field axis and with a kind of ratcheting motion where the dimers slide relative to each other while the whole configuration precesses on average.

As chaotic motion proceeds, fewer and fewer trajectories stay in chaotic state. Figures 6(a)–6(c) show the populations of trajectories remaining in the chaotic state at Mn = 1.06 and 1.253 (in the simulation) and at Mn = 1.5 (in the experiment). The simulations are performed over an ensemble of 500 different initial orientations of the chain. We run the simulations long enough (over 2000 field revolutions) that all 500 trajectories eventually leave the chaotic state and enter the periodic orbit. As can be seen in all three cases, the survival probability in the chaotic set, P_s, decays exponentially in time indicating a Poisson process. For the simulations, the decay time, τ, is on the order of a few hundred field revolutions and is indicated on the plot. We do not know how to compute this quantity from first principles yet, but the transition rates are much slower, and the chaotic lifetimes much longer than we had naively expected. Figure 6(a) shows a typical chaotic frequency, Mn = 1.253, where the ratio of cluster to molecule is approximately 1.5. Figure 6(b) shows a chaotic frequency, Mn = 1.06, where in addition to cluster and molecule, a third final periodic orbit is also possible. The third final state at Mn = 1.06 is a second kind of the special case described above. In experiments, sedimentation limits the observation time. As a result, we had to focus on very high Mn regime where the typical characteristic escape times are short (i.e., on the order of 10 to 100 field revolutions) and only clusters survive. Figure 6(c) shows the population in the chaotic state for 13 trajectories whose transitions we were able to capture during the course of the experiment.

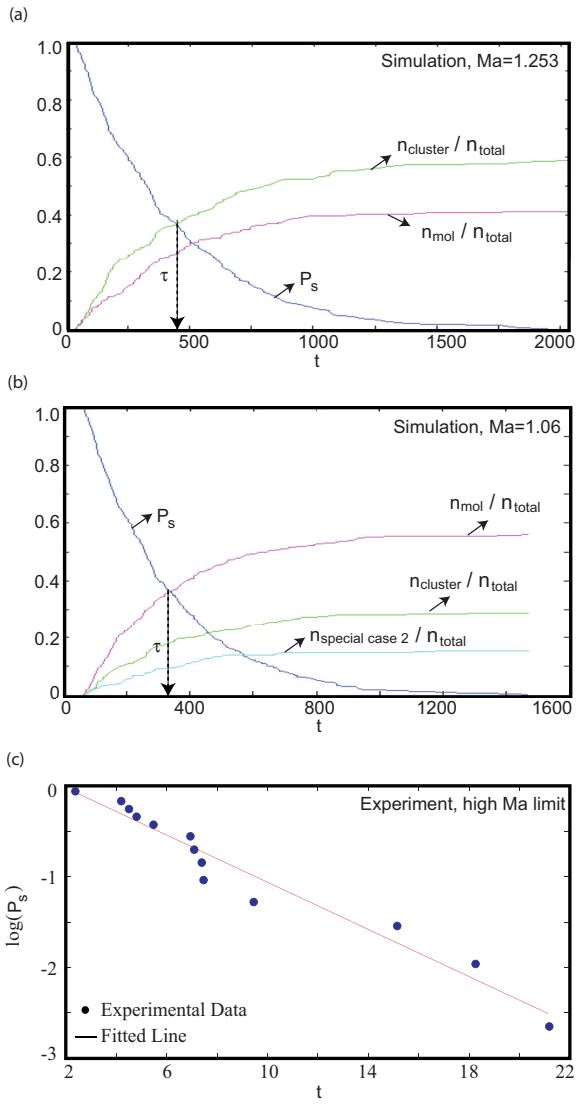

FIG. 6. Fraction of trajectories in chaotic and nonchaotic states vs time. (a) Mn = 1.253 (simulation) and (b) Mn = 1.06 (simulation). (c) High Mn limit (experiment). For (a) the dark blue curve which decreases monotonically corresponds to the fraction of chaotic states, the magenta to the fraction of molecules and the green to the fraction of clusters. For (b) the cyan curve corresponds to the fraction of trajectories in the second kind of special case orbits described in the text. In the experiment in (c) we observe escape only into clusters.

V. SUMMARY AND OUTLOOK

In summary, we presented results on the dynamics of four-particle chains of superparamagnetic particles subjected to a magnetic field rotating in a plane. We presented evidence for a regime of dynamical behavior in which the particles undergo a chaotic dynamics for a surprisingly long time before transitioning into a stable periodic orbit. We showed that the transition out of this chaotic regime and into the periodic orbit was consistent with a Poisson process in both experiment and simulation. It is worth noting that we are currently studying longer chains with a more sophisticated model including multibody magnetic and hydrodynamics interactions, and we observe similar behavior as we increase the number of particles in the chain.

In the simulation, we typically found either a closely packed cluster or a colloidal molecule with relatively high symmerty with some other periodic orbits of lower symmetry occasionally observed. In the experiment, although we found

evidence of some transient configurations with the structure of the molecules seen in the simulation, the only final periodic orbits we observed were closely packed clusters. We offer two possibilities as to why this is so. First, we may simply be running the experiment in a Mn regime where the molecules are less likely but not strictly forbidden. Although we have not systematically studied the Mn dependence of the transition rates, it is clear from Fig. 5 that the molecules disappear in favor of the clusters beyond a Mn of about 1.25. Second, in the experiment there is both particle-to-particle fluctuation in size and susceptibility and finite temperature. This disorder could destabilize the highly symmetric molecular orbit.

We have shown the survival probability distribution for remaining in the chaotic state for only one Mn in the experiment and only two Mn in the simulation. It would obviously be interesting to systematically explore the Mn dependence of the transition rates and, in particular, to study the relative proportion of clusters and molecules at various Mn. Also, the final periodic orbits we find in these $k_bT = 0$ simulations are essentially unconditionally stable; that is, they persist for as long as we are able to run the simulations. It would be interesting to check for the robustness of these periodic orbits at finite temperature. These studies are currently under way, and the preliminary results show a surprisingly important role for finite temperature even when k_bT is many orders of magnitude below the characteristic magnetostatic binding energy, ϵ_0. This might also help explain the absence of persistent molecular trajectories in the experiment.

We hope this work will stimulate other groups to search for periodic orbits with different, molecule-like, trajectories. The molecular trajectories could find applications in areas like photonics and mixing, but producing them reproducibly will require a fuller characterization and understanding of the Mn dependence of the various transition rates in the problem.

ACKNOWLEDGMENT

This material is based upon work supported by the National Science Foundation under Award No. DMR-1056564 and No. CPS-1329649.

[1] J. R. Melrose, Brownian dynamics simulation of dipole suspensions under shear: The phase diagram, Mol. Phys. **76**, 635 (1992).
[2] S. L. Biswal and A. P. Gast, Mechanics of semiflexible chains formed by poly (ethylene glycol)-linked paramagnetic particles, Phys. Rev. E **68**, 021402 (2003).
[3] S. L. Biswal and A. P. Gast, Rotational dynamics of semiflexible paramagnetic particle chains, Phys. Rev. E **69**, 041406 (2004).
[4] S. L. Biswal and A. P. Gast, Micromixing with linked chains of paramagnetic particles, Anal. Chem. **76**, 6448 (2004).
[5] S. Jäger and S. H. L. Klapp, Pattern formation of dipolar colloids in rotating fields: Layering and synchronization, Soft Matter **7**, 6606 (2011).
[6] S. Jäger, H. Schmidle, and S. H. L. Klapp, Nonequilibrium condensation and coarsening of field-driven dipolar colloids, Phys. Rev. E **86**, 011402 (2012).
[7] T. G. Kang, M. A. Hulsen, P. D. Anderson, J. M. J. den Toonder, and H. E. H. Meijer, Chaotic mixing induced by a magnetic chain in a rotating magnetic field, Phys. Rev. E **76**, 066303 (2007).
[8] T. G. Kang, M. A. Hulsen, J. M. J. den Toonder, P. D. Anderson, and H. E. H. Meijer, A direct simulation method for flows with suspended paramagnetic particles, J. Comput. Phys. **227**, 4441 (2008).
[9] M. E. Leunissen, H. R. Vutukuri, and A. V. Blaaderen, Directing colloidal self-assembly with biaxial electric fields, Adv. Mater. **21**, 3116 (2009).
[10] M. T. López-López, G. Vertelov, G. Bossis, P. Kuzhir, and J. D. G. Durán, New magnetorheological fluids based on magnetic fibers, J. Mater. Chem. **17**, 3839 (2007).
[11] J. E. Martin, R. A. Anderson, and C. P. Tigges, Simulation of the athermal coarsening of composites structured by a biaxial field, J. Chem. Phys. **108**, 7887 (1998).
[12] J. E. Martin, R. A. Anderson, and C. P. Tigges, Thermal coarsening of uniaxial and biaxial field-structured composites, J. Chem. Phys. **110**, 4854 (1999).
[13] J. E. Martin, R. A. Anderson, and R. L. Williamson, Generating strange magnetic and dielectric interactions: Classical molecules and particle foams, J. Chem. Phys. **118**, 1557 (2003).
[14] J. E. Martin and A. Snezhko, Driving self-assembly and emergent dynamics in colloidal suspensions by time-dependent magnetic fields, Rep. Prog. Phys. **76**, 126601 (2013).
[15] S. Melle, O. G. Calderón, M. A. Rubio, and G. G. Fuller, Rotational dynamics in dipolar colloidal suspensions: Video microscopy experiments and simulations results, J. Non-Newtonian Fluid Mech. **102**, 135 (2002).
[16] S. Melle, O. G. Calderón, M. A. Rubio, and G. G. Fuller, Microstructure evolution in magnetorheological suspensions governed by Mason number, Phys. Rev. E **68**, 041503 (2003).
[17] S. Melle and J. E. Martin, Chain model of a magnetorheological suspension in a rotating field, J. Chem. Phys. **118**, 9875 (2003).
[18] V. V. Murashov and G. N. Patey, Structure formation in dipolar fluids driven by rotating fields, J. Chem. Phys. **112**, 9828 (2000).
[19] Y. Nagaoka, H. Morimoto, and T. Maekawa, Dynamics of disklike clusters formed in a magnetorheological fluid under a rotational magnetic field, Phys. Rev. E **71**, 032502 (2005).
[20] N. Osterman, I. Poberaj, J. Dobnikar, D. Frenkel, P. Ziherl, and D. Babić, Field-Induced Self-Assembly of Suspended Colloidal Membranes, Phys. Rev. Lett. **103**, 228301 (2009).
[21] S. Y. Park, H. Handa, and A. Sandhu, Magneto-optical biosensing platform based on light scattering from self-assembled chains of functionalized rotating magnetic beads, Nano Lett. **10**, 446 (2009).
[22] P. Tierno, R. Muruganathan, and T. M. Fischer, Viscoelasticity of Dynamically Self-Assembled Paramagnetic Colloidal Clusters, Phys. Rev. Lett. **98**, 028301 (2007).
[23] T. Ukai, H. Morimoto, and T. Maekawa, Cluster-cluster aggregations of superparamagnetic particles in a rotational magnetic field, Phys. Rev. E **83**, 061406 (2011).
[24] A. K. Vuppu, A. A. Garcia, and M. A. Hayes, Video microscopy of dynamically aggregated paramagnetic particle chains in an applied rotating magnetic field, Langmuir **19**, 8646 (2003).

[25] A. Wiedenmann, U. Keiderling, K. Habicht, M. Russina, and R. Gähler, Dynamics of Field-Induced Ordering in Magnetic Colloids Studied by New Time-Resolved Small-Angle Neutron-Scattering Techniques, Phys. Rev. Lett. **97**, 057202 (2006).

[26] U. Jeong, X. Teng, Y. Wang, H. Yang, and Y. Xia, Superparamagnetic colloids: Controlled synthesis and niche applications, Adv. Mater. **19**, 33 (2007).

[27] F. Li, D. P. Josephson, and A. Stein, Colloidal assembly: The road from particles to colloidal molecules and crystals, Angew. Chem., Int. Ed. Engl. **50**, 360 (2011).

[28] H. Löwen, Colloidal dispersions in external fields: Recent developments, J. Phys.: Condens. Matter **20**, 404201 (2008).

[29] R. Soheilian, Y. S. Choi, A. E. David, H. Abdi, C. E. Maloney, and R. M. Erb, Toward accumulation of magnetic nanoparticles into tissues of small porosity, Langmuir **31**, 8267 (2015).

[30] J. W. Swan, J. L. Bauer, Y. Liu, and E. M. Furst, Directed colloidal self-assembly in toggled magnetic fields, Soft Matter **10**, 1102 (2014).

[31] J. H. E. Promislow and A. P. Gast, Magnetorheological fluid structure in a pulsed magnetic field, Langmuir **12**, 4095 (1996).

[32] K. Butter, P. H. Bomans, P. M. Frederik, G. J. Vroege, and A. P. Philipse, Direct observation of dipolar chains in ferrofluids in zero field using cryogenic electron microscopy, J. Phys.: Condens. Matter **15**, S1451 (2003).

[33] G. Cheng, D. Romero, G. T. Fraser, and A. R. H. Walker, Magnetic-field-induced assemblies of cobalt nanoparticles, Langmuir **21**, 12055 (2005).

[34] D. Liu, M. R. Maxey, and G. E. Karniadakis, Simulations of dynamic self-assembly of paramagnetic microspheres in confined microgeometries, J. Micromech. Microeng. **15**, 2298 (2005).

[35] J. E. Martin, Theory of strong intrinsic mixing of particle suspensions in vortex magnetic fields, Phys. Rev. E **79**, 011503 (2009).

[36] J. E. Martin, L. Shea-Rohwer, and K. J. Solis, Strong intrinsic mixing in vortex magnetic fields, Phys. Rev. E **80**, 016312 (2009).

[37] I. Petousis, E. Homburg, R. Derks, and A. Dietzel, Transient behavior of magnetic micro-bead chains rotating in a fluid by external fields, Lab Chip **7**, 1746 (2007).

[38] C. E. Sing, L. Schmid, M. F. Schneider, T. Franke, and A. Alexander-Katz, Controlled surface-induced flows from the motion of self-assembled colloidal walkers, Proc. Natl. Acad. Sci. USA **107**, 535 (2010).

[39] J. Jordanovic and S. H. L. Klapp, Field-Induced Layer Formation in Dipolar Nanofilms, Phys. Rev. Lett. **101**, 038302 (2008).

[40] Y. Gao, M. A. Hulsen, T. G. Kang, and J. M. J. den Toonder, Numerical and experimental study of a rotating magnetic particle chain in a viscous fluid, Phys. Rev. E **86**, 041503 (2012).

[41] B. A. Grzybowski, X. Jiang, H. A. Stone, and G. M. Whitesides, Dynamic, self-assembled aggregates of magnetized, millimeter-sized objects rotating at the liquid-air interface: Macroscopic, two-dimensional classical artificial atoms and molecules, Phys. Rev. E **64**, 011603 (2001).

[42] B. A. Grzybowski, H. A. Stone, and G. M. Whitesides, Dynamic self-assembly of magnetized, millimetre-sized objects rotating at a liquid–air interface, Nature (London) **405**, 1033 (2000).

[43] D. Du, F. Toffoletto, and S. L. Biswal, Numerical calculation of interaction forces between paramagnetic colloids in two-dimensional systems, Phys. Rev. E **89**, 043306 (2014).

[44] E. E. Keaveny and M. R. Maxey, Modeling the magnetic interactions between paramagnetic beads in magnetorheological fluids, J. Comput. Phys. **227**, 9554 (2008).

[45] A. Malevanets and R. Kapral, Mesoscopic model for solvent dynamics, J. Chem. Phys. **110**, 8605 (1999).

[46] J. J. Weis, Simulation of quasi-two-dimensional dipolar systems, J. Phys.: Condens. Matter **15**, S1471 (2003).

[47] H. Zhang and M. Widom, Field-induced forces in colloidal particle chains, Phys. Rev. E **51**, 2099 (1995).

[48] E. Ott, *Chaos in Dynamical Systems* (Cambridge University Press, Cambridge, 2002).

[49] F. Argoul, J. Huth, P. Merzeau, A. Arneodo, and H. L. Swinney, Experimental evidence for homoclinic chaos in an electrochemical growth process, Physica D (Amsterdam) **62**, 170 (1993).

[50] A. Brandstäter, J. Swift, H. L. Swinney, A. Wolf, J. D. Farmer, E. Jen, and P. J. Crutchfield, Low-Dimensional Chaos in a Hydrodynamic System, Phys. Rev. Lett. **51**, 1442 (1983).

[51] A. E. Motter, M. Gruiz, G. Károlyi, and T. Tél, Doubly Transient Chaos: Generic form of Chaos in Autonomous Dissipative Systems, Phys. Rev. Lett. **111**, 194101 (2013).

[52] See Supplemental Material at http://link.aps.org/supplemental/10.1103/PhysRevE.97.032601 for movies from the simulations and experiments.

[53] C. E. Maloney and D. J. Lacks, Energy barrier scalings in driven systems, Phys. Rev. E **73**, 061106 (2006).